Research Article | Vol. 33, No. 11 / 2 Jun 2025 / Optics Express 23260
Optics EXPRESS

Experimental Kerr constant determination for pure blue phase liquid crystal: oblique incidence in a reflective vertical field switching cell

SUMANYU CHAUHAN,[1,2,*] MARKUS WAHLE,[1] DIETER CUYPERS,[2] GRIGORY LAZAREV,[1] AND HERBERT DE SMET[2]

[1] *Optical Technology Laboratory, Huawei Munich Research Center, 80992 Munich, Germany*
[2] *Centre for Microsystems Technology (CMST), IMEC and Ghent University, 9052 Ghent, Belgium*
[*] *sumanyu.chauhan@huawei.com*

Abstract: The use of blue phase liquid crystals (BPLCs) in spatial light modulators (SLMs) offer advantages over traditional nematic LCs due to their polarization-independent behavior. We demonstrate a simplified reflection-mode setup similar to liquid crystal on silicon (LCoS) technology to evaluate BPLC performance. Using a vertical field switching (VFS) reflective cell with pure BPLC, we achieve phase modulation without complex cell fabrication methods typically needed for BPLCs in VFS configurations. Our measurements validate the setup's effectiveness in characterizing BPLC electro-optic response. The measured Kerr constant of $K \approx 4.4\,\mathrm{nm\,V^{-2}}$ demonstrates this approach's viability for developing BPLC-based SLMs.

1. Introduction

Spatial light modulators are electro-optical devices designed to manipulate light properties, such as intensity, phase, or polarization. They are crucial in applications ranging from image projection and display to lithography and optical manipulation [1–3]. In telecommunications, the primary function of LC or LCoS-based SLMs is diffractive beam steering, beam-splitting and beam attenuation by means of spatial phase modulation [4]. Liquid crystals [5] are a popular choice for SLMs due to their ability to reorient molecules in response to an electric field. The optical anisotropy of LC molecules induces varying phase delays for the incident light depending on the orientation of the molecules. By controlling the electric field across different regions of the LC layer, the SLM creates the desired pattern of phase shifts. However, conventional SLMs using uniaxial LCs are sensitive to the light's polarization, meaning that the output polarization and phase shift depends on the initial polarization state. This limitation can cause unwanted polarization modulation if the light is not perfectly aligned with the LC's optic axis, requiring additional optical elements, like polarizers, waveplates or other polarization diversity components [6], which increase system complexity and cost. Furthermore, non-ideal polarization handling can lead to performance degradation and reduced overall efficiency.

Cubic blue-phase liquid crystals (BPLCs) are a promising material for LCoS SLMs because of their unique electro-optic properties. Their self-assembled double-twist structure in a cubic geometry [7–11] creates inherent macroscopic anisotropy, enabling uniform phase shift across all light polarizations. BPLCs exhibit little to no anisotropy in the off-state [12]. These properties of BPLC overcomes the limitations of nematic liquid crystals (NLCs) and eliminates the need for additional polarization control elements, leading to simpler and more compact optical schemes. BPLCs further provide fast, sub-millisecond switching times, making them ideal for applications requiring rapid light modulation [13].

#560601 https://doi.org/10.1364/OE.560601
Journal © 2025 Received 25 Mar 2025; revised 28 Apr 2025; accepted 29 Apr 2025; published 27 May 2025

Optics EXPRESS

Most electro-optics characterization studies of BPLCs typically use polymer-stabilized BPLC (PS-BPLC) in in-plane switching (IPS) mode [14], with a laterally oriented electric field. Besides the obvious polarization dependence (induced optic axis is parallel to the E-field and perpendicular to the light propagation direction), the IPS mode suffers from high operating voltages and hysteresis (memory effect). The high driving voltage is needed because the electric field gets concentrated near the plane of the electrodes, and does not penetrate deeply into the bulk of the LC. Additionally, the non-uniform electric field in IPS can cause lattice deformation near the edges, leading to hysteresis [15,16]. Several modified IPS structures have been proposed to address these issues, such as protrusion electrodes and corrugated designs [17,18]. While these methods help reduce the operating voltage, they also complicate the manufacturing process.

Vertical field switching (VFS) offers an alternative measurement approach. A prism-array based VFS employs two prism array sheets attached to top and bottom substrates and a BPLC layer between them. The bottom prism sheet redirects normal incident light to oblique angles, allowing the light to experience phase retardation (due to the difference in ordinary and extraordinary refractive indices) as it passes through the BPLC layer under vertical electric field. The top prism then redirects the light back to normal viewing direction. The main technical challenge lies in precise prism sheet fabrication and alignment. The large oblique incidence VFS reduces operating voltage and eliminates hysteresis. Another method which uses immersion of VFS PS-BPLC cells in glycerol leads to a cumbersome and impractical setup [19–23]. Unlike IPS, VFS utilizes a uniform electric field, enabling lower voltage and faster response time through a thin cell gap. This study presents a novel, simplified method for reflection-mode BPLC SLMs.

We propose a reflective VFS cell with pure BPLC without polymer scaffolding. Our experimental setup (see Fig. 1) comprises a polarizer, a BPLC cell rendered reflective with aluminum coating, and a polarimeter. This setup exhibits effective phase difference in reflection mode. This design simplifies characterization of BPLC SLMs without the need for microfabricated prismatic structures or immersion in glycerol medium as proposed in earlier studies. Furthermore, an analytical Kerr model(s) is used to determine the Kerr constant by fitting the experimental data.

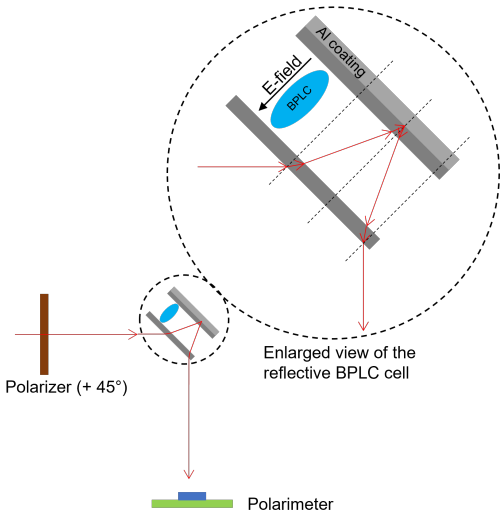

Fig. 1. Schematic of the experimental setup for measuring the phase modulation of BPLC in a reflective VFS cell.

Optics EXPRESS

2. Experimental setup

The BPLC mixture consisted of nematic liquid crystal blend HTG135400-100 (Jiangsu Hecheng Display Technology Co., Ltd.) with electrical and optical properties: $\varepsilon_{\parallel} = 49.6$, $\varepsilon_{\perp} = 11.5$, $\tilde{n}_e = 1.67$, and $\tilde{n}_o = 1.51$, where $\tilde{n}_o$ and $\tilde{n}_e$ represent ordinary and extraordinary refractive indices. To enhance device lifetime, 3.04% chiral dopant S5011 with high helical twisting power (HTP = 126 μm^{-1}) was added to maintain blue phase stability [24].

The vertical field switching (VFS) cells comprised ITO-coated glass substrates with a 6 µm cell gap and 10 mm × 10 mm clear aperture. Substrates were treated with polyimide (PI) layer and rubbed for homogeneous alignment. A 1 µm aluminum layer deposited on the bottom substrate enabled reflection-mode operation, mimicking LCoS devices. This combination of BPLC material, alignment layers, and cell structure has been previously characterized for monodomain alignment [25] and phase transition thresholds [26].

For phase modulation characterization, the cell was mounted on a Linkam LTS 120 heat stage with T-96 temperature controller (temperature stability and accuracy < 0.01 °C) maintained at 73 °C. This BPLC mixture exists within a temperature range of 71 °C - 74 °C. A 1 kHz square wave signal drove the cell below the blue phase to N* phase transition threshold [26].

The BPLC morphology remained stable throughout testing under precise temperature control, as verified by microscopic observation. Measurements were taken once per test as hysteresis was not the focus of this study. The material was cooled from its isotropic phase to the BPLC state before voltage application for phase modulation. Phase difference values proved repeatable across multiple isotropic-BP-voltage application cycles.

Figure 1 shows the experimental configuration for measuring phase modulation. A collimated 633 nm laser beam was directed at 45° incidence to the reflective cell surface. The polarizer axis was oriented at 45° relative to the incidence plane. The cell's surface normal lies in the incidence plane at 45° to the incident beam. Applied voltage induced elongation of the BPLC's index ellipsoid along the electric field direction. Light polarized parallel to the incidence plane (TM mode) encountered effective refractive index $n'(E)$ of the BPLC index ellipsoid, while perpendicularly polarized light (TE mode) experienced ordinary refractive index $n_o(E)$. Phase difference measurements were obtained using a Thorlabs PAX1000VIS polarimeter with ±0.25° accuracy.

3. Modeling techniques for oblique incidence in anisotropic media

For LCs in isotropic phase, the isotropic refractive index $\tilde{n}_{\text{iso}}$ is given by [27,28]:

$$\tilde{n}_{\text{iso}} = \sqrt{\frac{2\tilde{n}_o^2 + \tilde{n}_e^2}{3}}, \tag{1}$$

where $\tilde{n}_o$ and $\tilde{n}_e$ represent the ordinary and extraordinary refractive indices of the nematic mixture. For typical nematic liquid crystals with $\tilde{n}_o \approx 1.50$ and $\tilde{n}_e \approx 1.70$, Eq. (1) can be approximated by the average refractive index $\langle \tilde{n} \rangle$ of the nematic liquid crystal.

Similarly, BPLC in its optically isotropic state (i.e., in the absence of an external electric field) has an isotropic refractive index n_{iso} that can be approximated by the average of the refractive index ellipsoid $\langle n \rangle$:

$$n_{\text{iso}} \approx \langle n \rangle = \frac{2\tilde{n}_o + \tilde{n}_e}{3}. \tag{2}$$

3.1. Electric field-dependent behavior of BPLCs

For BPLCs, the absence of an electric field results in optically isotropic behavior. For BPLCs made with positive dielectric anisotropy nematics mixtures, upon applying a voltage, the index ellipsoid elongates along the direction of applied field and shortens along the direction perpendicular to

Optics EXPRESS

the applied electric field, optical axis of the index ellipsoid of BPLC remains aligned with the electric field. In VFS geometry, for nematic LCs, the optic axis rotates with increasing voltage while $\tilde{n}_o$ and $\tilde{n}_e$ remain constant as depicted in the schematic shown in Fig. 2(a), the effective refractive index of nematic accounts for light oblique angles. However, for BPLCs, both $n_o(E)$ and $n_e(E)$ vary with the electric field, as well as the effective refractive index (see Eq. (6)), which accounts for light at oblique angles as depicted in the schematic shown in Fig. 2(b).

(a) Nematic LC in VFS geometry.

(b) BPLC in VFS geometry.

Fig. 2. Evolution of optical indicatrix in VFS cell geometry for nematic and blue-phase liquid crystals.

The electrically induced birefringence of BPLCs is defined as:

$$\Delta n(E)_{\text{ind}} = n_e(E) - n_o(E) \tag{3}$$

where the ordinary and extraordinary refractive indices are:

$$n_o(E) = n_{\text{iso}} - \frac{\Delta n(E)_{\text{ind}}}{3} \tag{4}$$

$$n_e(E) = n_{\text{iso}} + \frac{2\Delta n(E)_{\text{ind}}}{3} \tag{5}$$

The effective refractive index $n'(E)$ is given by [27]:

$$n'(E) = \frac{n_o(E)n_e(E)}{\sqrt{n_o^2(E)\sin^2\phi + n_e^2(E)\cos^2\phi}} \tag{6}$$

where ϕ is the angle between the LC molecule's optic axis and the light's wave vector.

3.2. Limitation of refractive index in BPs

To derive the refractive index change in BPLC, δn, we begin with its definition:

$$\delta n = n_{\text{iso}} - n_o(E) \tag{7}$$

$$\delta n = \langle n \rangle - n_o(E) \tag{8}$$

Substituting the expression for the average refractive index $\langle n \rangle$ and simplifying yields :

$$\delta n = \frac{1}{3}\big(n_e(E) - n_o(E)\big) \tag{9}$$

The saturated refractive index change can be derived as:

$$\delta n_{\text{sat}} = \frac{\Delta\tilde{n}}{3} \tag{10}$$

where $\Delta\tilde{n}$ is the birefringence of the nematic host. From Eq. (10), it is evident that the maximum birefringence induced by the Kerr effect, δn_{sat}, due to refractive index change, δn, of BPLC is limited to one-third of the birefringence of the constituent nematic, $\Delta\tilde{n}$. This is one of the fundamental performance limiting factors of BPLCs.

Optics EXPRESS

3.3. Kerr effect in BPLCs

The isotropic-to-anisotropic transition in BPLCs (as illustrated in Fig. 2(b)) is governed by the Kerr effect, with field-induced birefringence described using the Kerr model defined by Wu et. al [28]:

$$\Delta n_{\text{ind}} = n_e(E) - n_o(E) = \lambda K E^2 \tag{11}$$

where λ is the wavelength of the incident light, K is the Kerr constant, and E is the amplitude of the electric field. To address unrealistic divergence at high fields, a saturation field (E_s) and exponential convergence is introduced to the Kerr model, and the exponential Kerr model is then described as :

$$\delta n = \delta n_{\text{sat}} \left(1 - \exp\left(-\left(\frac{E}{E_s}\right)^2\right)\right) \tag{12}$$

This improved model ensures a smooth saturation transition for high-field birefringence [28].

3.4. Phase shift equations

The phase shift for the transverse magnetic (TM) mode, where light polarization is parallel to the plane of incidence, is given by:

$$\Phi_{\text{TM}} = \frac{2d}{\cos(\theta_{\text{BP}})} \frac{2\pi}{\lambda} n'(\Delta n, \theta_{\text{BP}}) \tag{13}$$

The phase shift for the transverse electric (TE) mode, where light polarization is perpendicular to the plane of incidence, is expressed as:

$$\Phi_{\text{TE}} = \frac{2d}{\cos(\theta_{\text{BP}})} \frac{2\pi}{\lambda} n_o(\Delta n) \tag{14}$$

The general phase shift, for an oblique incidence angle, $\Delta\phi(\Delta n, \theta_{\text{BP}})$, accounts for both the effective refractive index and the ordinary refractive index, given by:

$$\Delta\phi(\Delta n, \theta_{\text{BP}}) = \frac{2d}{\cos(\theta_{\text{BP}})} \frac{2\pi}{\lambda} [n'(\Delta n, \theta_{\text{BP}}) - n_o(\Delta n)] \tag{15}$$

where d is the thickness of the cell, θ_{BP} is the angle inside BPLC, λ is the wavelength of light, $n'(\Delta n, \theta_{\text{BP}})$ is the effective refractive index of BPLC, and $n_o(\Delta n)$ is the ordinary refractive index of BPLC.

4. Discussion

This study uses simple setup for measurement of phase difference of BPLCs in a VFS cell. Later on using simulations, measurements and curve fitting of the experimental data to the standard Kerr model, and the exponential Kerr model, Kerr constant for the given BPLC lattice orientation is determined. The simulation initializes with a cell gap of 6 μm, a maximum applied voltage of 14 V_{rms}, and a light wavelength of 633 nm. The initial Kerr constant is set to 0.1 nm V^{-2}. Other parameters include extraordinary and ordinary refractive indices of constituent nematics blend as 1.67 and 1.51, respectively, a refractive index of 1.0003 for air and 1.51 for glass, and an incidence angle of 45 degrees at the glass-air interface. The maximum applied voltage of 14 V_{rms} is deliberately chosen to prevent damage of the BPLC lattice or voltage induced phase change of the BPLC [26], as shown in the Fig. 3. While these voltages are very high for integrating BP into a commercial LCoS backplane limited by CMOS electronics, this study's aim is not material optimization but a demonstration of a simple method to characterize a BP SLM in a VFS mode cell.

Optics EXPRESS

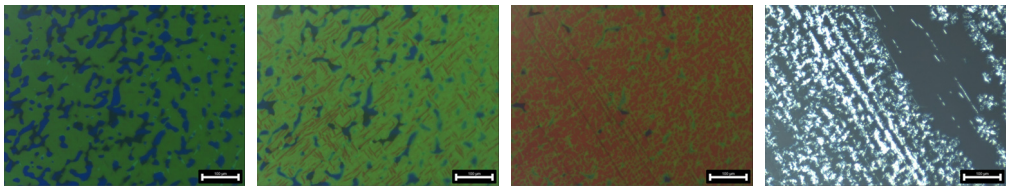

(a) 6 µm (ST), 0.0 V_{rms} (b) 6 µm (ST), 7.0 V_{rms} (c) 6 µm (ST), 10.0 V_{rms} (d) 6 µm (ST), 15.5 V_{rms}

Fig. 3. POM images of E-field induced phase transition in BP 6 µm glass cells, surface-treated (ST) for homogeneous alignment. The test temperature was 73.0 °C. Scale bar: 100 µm.

To simulate these models and determine the Kerr constant, it is important to determine the saturation values of electric field in BPLC. These saturation values are used directly into the extended and exponential Kerr models. The exponential Kerr model uses saturation field value, ensuring a smooth, exponential transition to saturation. The birefringence in this model asymptotically approaches its maximum value as the applied electric field increases.

The simulation compares various Kerr models by first generating a voltage array from 0 to 14 V_{rms} in 0.1 V increments. For each voltage step, the corresponding electric field is calculated, and the induced birefringence is computed using the standard Kerr, extended Kerr, and exponential Kerr models, the latter two incorporating previously determined saturation values [28]. These birefringence values are then used to calculate the ordinary ($n_o(E)$), extraordinary ($n_e(E)$), and average ($\langle n \rangle$) refractive indices via Eq. (4), Eq. (5), and Eq. (2), respectively. Subsequently, the phase shift experienced by orthogonally polarized light (TM and TM modes, see Eq. (13) and Eq. (14)) is determined, then the phase difference is accounting for oblique incidence is determined using Eq. (15). This iterative process yields phase difference arrays as a function of voltage for each model. Simulations with varying Kerr constants (K = 0.1 nm V^{-2}, Fig. 4(a); K = 4 nm V^{-2}, Fig. 4(b); K = 25 nm V^{-2}, Fig. 4(c)) reveal negligible differences between the standard and extended Kerr models for small K values. However, for larger K values, a significant deviation emerges among the three models, indicating that the exponential Kerr model offers a more accurate prediction of phase difference at higher electric field values, making it better suited for curve fitting and experimental data comparison.

The incident beam undergoes multiple refractions and reflections as it traverses the cell's optical stack, as illustrated in Fig. 1. These are: (1) refraction from air into the first glass substrate; (2) refraction from the glass substrate into the BPLC, where Snell's law and the average BPLC refractive index (defined in Eq. (2)) govern the refractive angle, and the beam splits into its TE and TM components; (3) refraction from the BPLC into the second glass substrate; (4) reflection from the Al coating on the back surface of the second glass substrate; (5) refraction from the second glass substrate back into the BPLC (after reflection from the cell's rear reflective coating); (6) refraction from the BPLC back into the first glass substrate; and (7) refraction from the first glass substrate into the air. Finally, a polarimeter measures the cumulative phase difference accumulated between the TE and TM waves after this complex optical path.

The Kerr constant (K) for the BPLC lattice orientation is determined via optimization, comparing simulated and experimental phase differences from polarimeter measurements. The procedure minimizes the mean absolute deviation (MAD) between simulated and raw experimental data. It must be emphasized that the Kerr constant is temperature dependent [29] and anisotropic [30,31]. It is to be noted that the the usual temperatures inside telecommunication equipment is around 65°C which is not too far from the test temperature used in this study.

This optimization procedure identifies the Kerr constant that best reproduces the experimental voltage-dependent phase differences, without using any data interpolation. Through the iterative

Optics EXPRESS

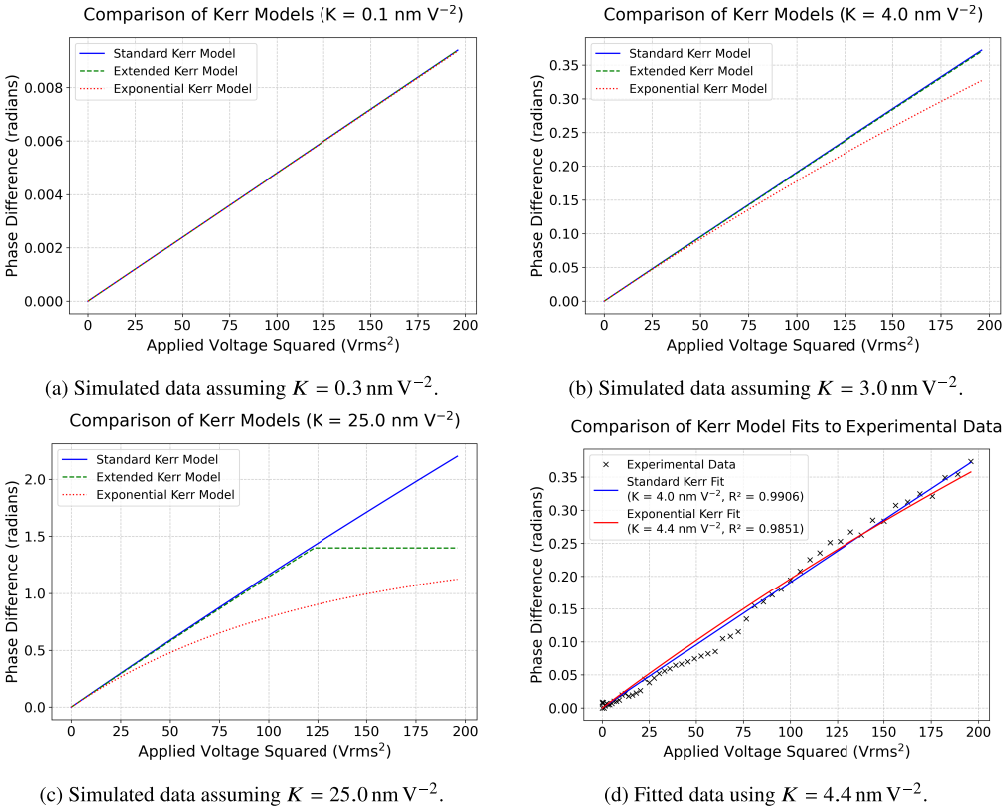

(a) Simulated data assuming $K = 0.3\,\mathrm{nm\,V^{-2}}$.

(b) Simulated data assuming $K = 3.0\,\mathrm{nm\,V^{-2}}$.

(c) Simulated data assuming $K = 25.0\,\mathrm{nm\,V^{-2}}$.

(d) Fitted data using $K = 4.4\,\mathrm{nm\,V^{-2}}$.

Fig. 4. Combined figures of simulated and fitted data. (a), (b), and (c) show simulated data for phase difference using different Kerr models and constants in a 6 µm VFS cell. (d) shows fitted data and Kerr constant values for standard Kerr fit and exponential Kerr fit. The setup used is described in Fig. 1.

minimization of the MAD, we determined the optimal Kerr constant for the specific BPLC lattice orientation [30,31]. Using the standard Kerr model, we obtained $K = 4.0$ nm V^{-2}, while the exponential Kerr model yielded $K = 4.4$ nm V^{-2}, as illustrated in Fig. 4(d). The exponential Kerr model resulted in a value of K that differs by 10% compared to the standard Kerr model. This discrepancy can be attributed to the inherent characteristics of the exponential model, which provides a more realistic representation of birefringence (and consequently phase difference) at higher voltages and larger values of K, as demonstrated by simulations in Fig. 4(b) and Fig. 4(c). As a comparison, highest Kerr constant values of $K = 13.7$ nm V^{-2} have been reported in polymer stabilized BPLC systems without alignment layers [32].

5. Conclusion

This work demonstrates a simplified, reflection-mode vertical field switching (VFS) configuration for characterizing pure blue-phase liquid crystals (BPLCs). This configuration, analogous to a liquid crystal on silicon (LCoS) device, utilizes a reflective aluminum coating on one substrate. This allows direct measurement of the voltage-dependent phase shift of a BPLC mixture without requiring complex components and cell fabrication (e.g., prismatic structures, immersion media, protruding electrodes in IPS cell, or polymer stabilization). Experimental measurements, combined with simulations employing an exponential Kerr model (crucial for

Optics EXPRESS

capturing saturation at higher voltages), were used to determine the Kerr constant. By minimizing the mean absolute deviation between measured and simulated phase differences, we found the Kerr constant for the specific BPLC lattice orientation within our VFS cell to be: $K \approx 4.4\,\text{nm}\,\text{V}^{-2}$. This simplified reflective VFS configuration offers advantages for BPLC-based spatial light modulator (SLM) development. The elimination of complex fabrication and additional polarization optics potentially enables simpler, more compact, and lower-voltage SLM designs. Future research will focus on investigating the Kerr constant's dependence on BPLC lattice orientation through the use of different alignment layers.

Disclosures. The authors declare no conflicts of interest.

Data availability. Data underlying the results presented in this paper are not publicly available at this time but may be obtained from the authors upon reasonable request.

References

1. A. D. Fisher, "A review of spatial light modulators," in *Topical Meeting on Optical Computing*, (Optica Publishing Group, 1985), p. TuC1.
2. H. Gao, F. Xu, J. Liu, *et al.*, "Holographic three-dimensional virtual reality and augmented reality display based on 4k-spatial light modulators," Appl. Sci. **9**(6), 1182 (2019).
3. G. Kim, S. Kim, H. Kim, *et al.*, "Metasurface-empowered spectral and spatial light modulation for disruptive holographic displays," Nanoscale **14**(12), 4380–4410 (2022).
4. G. Lazarev, A. Hermerschmidt, S. Krüger, *et al.*, "Lcos spatial light modulators: trends and applications," Optical Imaging and Metrology: Advanced Technologies pp. 1–29 (2012).
5. P. J. Collings, *Liquid crystals: nature's delicate phase of matter* (Princeton University Press, 2002).
6. Z. Zhu, Y. Wen, J. Li, *et al.*, "Metasurface-enabled polarization-independent LCoS spatial light modulator for 4K resolution and beyond," Light: Sci. Appl. **12**(1), 151 (2023).
7. P. P. Crooker, "Blue phases," Chirality in liquid crystals pp. 186–222 (2001).
8. H. Stegemeyer, T. Blümel, K. Hiltrop, *et al.*, "Thermodynamic, structural and morphological studies on liquid-crystalline blue phases," Liq. Cryst. **1**(1), 3–28 (1986).
9. D. C. Wright and N. D. Mermin, "Crystalline liquids: the blue phases," Rev. Mod. Phys. **61**(2), 385–432 (1989).
10. D. Johnson, J. Flack, and P. Crooker, "Structure and properties of the cholesteric blue phases," Phys. Rev. Lett. **45**(8), 641–644 (1980).
11. P. P. Crooker, "Plenary lecture. the blue phases. a review of experiments," Liq. Cryst. **5**(3), 751–775 (1989).
12. S. Chauhan, M. Wahle, G. Lazarev, *et al.*, "An experimental study of optical anisotropy of blue-phase liquid crystals as a function of alignment layers," in *Optical Components and Materials XX*, vol. 12417 (SPIE, 2023), pp. 223–229.
13. Y.-H. Lin, H.-S. Chen, H.-C. Lin, *et al.*, "Polarizer-free and fast response microlens arrays using polymer-stabilized blue phase liquid crystals," Appl. Phys. Lett. **96**(11), 113505 (2010).
14. Y. Chen and S.-T. Wu, "Recent advances on polymer-stabilized blue phase liquid crystal materials and devices," J. Appl. Polym. Sci. **131**(15), 1 (2014).
15. Y.-F. Lan, C.-Y. Tsai, J.-K. Lu, *et al.*, "Mechanism of hysteresis in polymer-network stabilized blue phase liquid crystal," Polymer **54**(7), 1876–1879 (2013).
16. K.-M. Chen, S. Gauza, H. Xianyu, *et al.*, "Hysteresis effects in blue-phase liquid crystals," J. Disp. Technol. **6**(8), 318–322 (2010).
17. Y. Guo, Y. Wang, C. Zhang, *et al.*, "Low voltage blue-phase liquid crystal display with insulating protrusion sandwiched between dual-layer electrodes," Liq. Cryst. **46**(4), 523–534 (2019).
18. Y. Guo, Y. Wang, C. Zhang, *et al.*, "Blue-phase liquid crystal display with insulating protrusion," Liq. Cryst. **45**(11), 1585–1593 (2018).
19. Y. Li, S. Huang, P. Zhou, *et al.*, "Polymer-stabilized blue phase liquid crystals for photonic applications," Adv. Mater. Technol. **1**(8), 1600102 (2016).
20. H.-C. Cheng, J. Yan, T. Ishinabe, *et al.*, "Blue-phase liquid crystal displays with vertical field switching," J. Disp. Technol. **8**(2), 98–103 (2012).
21. H.-C. Cheng, J. Yan, T. Ishinabe, *et al.*, "Vertical field switching for blue-phase liquid crystal devices," Appl. Phys. Lett. **98**(26), 261102 (2011).
22. Y.-H. Kim, S.-T. Hur, K.-w. Park, *et al.*, "23.3: A vertical-field-driven polymer-stabilized blue phase liquid crystal displays," in *SID Symposium Digest of Technical Papers*, vol. 42 (Wiley Online Library, 2011), pp. 298–301.
23. Y.-H. Kim, S.-T. Hur, C.-S. Park, *et al.*, "A vertical-field-driven polymer-stabilized blue phase liquid crystal mode to obtain a higher transmittance and lower driving voltage," Opt. Express **19**(18), 17427–17438 (2011).
24. P. Joshi, J. De Smet, X. Shang, *et al.*, "Long term stability of polymer stabilized blue phase liquid crystals," J. Disp. Technol. **11**(9), 703–708 (2015).
25. S. Chauhan, D. Cuypers, M. Wahle, *et al.*, "Nematic host and alignment layer dependence on monodomain formation in the liquid crystal blue phase," Opt. Mater. Express **15**(1), 11–20 (2025).

Optics EXPRESS

26. S. Chauhan, M. Wahle, D. Cuypers, *et al.*, "Effect of surface alignment on electric-field-induced phase transitions in blue phases," APL Mater. **12**(10), 101114 (2024).
27. D.-K. Yang and S.-T. Wu, *Fundamentals of liquid crystal devices* (John Wiley & Sons, 2014).
28. J. Yan, H.-C. Cheng, S. Gauza, *et al.*, "Extended kerr effect of polymer-stabilized blue-phase liquid crystals," Appl. Phys. Lett. **96**(7), 071105 (2010).
29. L. Tian, J. W. Goodby, V. Görtz, *et al.*, "The magnitude and temperature dependence of the kerr constant in liquid crystal blue phases and the dark conglomerate phase," Liq. Cryst. **40**(11), 1446–1454 (2013).
30. H. Tone, H. Yoshida, S. Yabu, *et al.*, "Effect of anisotropic lattice deformation on the kerr coefficient of polymer-stabilized blue-phase liquid crystals," Phys. Rev. E **89**(1), 012506 (2014).
31. Y. Kawata, H. Yoshida, S. Tanaka, *et al.*, "Anisotropy of the electro-optic kerr effect in polymer-stabilized blue phases," Phys. Rev. E **91**(2), 022503 (2015).
32. L. Rao, J. Yan, S.-T. Wu, *et al.*, "A large kerr constant polymer-stabilized blue phase liquid crystal," Appl. Phys. Lett. **98**(8), 081109 (2011).